RSC Advances

ROYAL SOCIETY OF CHEMISTRY

www.rsc.org/advances

Modeling and Optimization of Catalytic Performance of SAPO-34 Nanocatalysts Synthesized Sonochemically Using a new hybrid of Non-dominated Sorting Genetic Algorithm-II based Artificial Neural Networks (NSGA-II – ANN)

Sima Askari[1]; Rouein Halladj*; Mohammad Javad Azarhoosh[1]

1: Faculty of Chemical Engineering, Amirkabir University of Technology (Tehran Polytechnic), P.O. Box 15875-4413, Hafez Ave., Tehran, Iran.

Abstract

Effects of ultrasound-related variables on catalytic properties of sonochemically prepared SAPO-34 nanocatalyst in methanol to olefins (MTO) reactions were investigated. The different catalytic behaviors are observed which can be explained by the differences in the catalysts physicochemical properties affected by ultrasonic (US) power intensity, sonication temperature, irradiation time and sonotorode size. This result confirms that the activity of SAPO-34 catalysts improves with the rise in US power, time and temperature. In order to find a catalyst with maximum conversion of methanol, maximum light olefins content and maximum lifetime, the hybrid of non-dominated sorting genetic algorithm-II based artificial neural networks (NSGA-II – ANN) was used. The multilayer feed forward neural networks with back-propagation structures were implemented using different training rules in the neural networks approach to relate the ultrasound-related variables and the catalytic performance of SAPO-34 catalysts. A comparison between experimental and artificial neural network (ANN) values indicates that the ANN model with a 3-10-3 structure using the Bayesian regulation training rule has the best fit and can be used as a fitness evaluation inside the non-dominated sorting genetic algorithm-II (NSGA-II). Also, the multiple linear regressions (MLR) was used to predict these objective functions. The results indicate a poor fit for the objective functions with low coefficient of determination. This confirms the ANN technique is more effective than the traditional statistical-based prediction models. Finally, this ANN model was linked to the NSGA-II and Pareto-optimal solutions were determined by NSGA-II.

Keywords: SAPO-34 nanocatalysts; sonochemical synthesis; ultrasound-related variables; MTO reaction; artificial neural network; Non-dominated Sorting Genetic Algorithm-II.

*: Corresponding author, Rouein. Halladj, halladj@aut.ac.ir
Tel number: 00982164543151.
Fax number: 00982166405847.

1. Introduction

Because of the growing demand for light olefins and the shortage of petroleum resources in the future, the MTO technology, regarded as an alternative process for the production of light olefins from nonpetroleum sources without using a large amount of energy, has received strong significant academic and industrial attention. SAPO-34 catalyst shows an exceptional selectivity for lower olefins and the complete conversion of methanol in the MTO reaction, although it is rapidly deactivated by coke, which completely blocks the internal channels of the SAPO-34 crystals [1]. Using SAPO-34 catalyst with small crystallite size enhances the accessibility of methanol into its cages, resulting in better catalytic performance [2-4]. Since the diffusion of methanol in the SAPO-34 catalyst is limited by its small cages, only some cages near the external surface are active in the MTO reaction [5], therefore the effectiveness of the SAPO-34 catalyst is improved by reducing its crystallite size [4].

The importance of nanoparticles, especially nanocatalysis and their uses in different industries has attracted many researches. The materials in nano-scale show different characteristics in comparison with their bulk state [6, 7]. A great number of investigations about the effect of crystal size show that the best performance for SAPO-34 catalysts are of sizes less than 500 nm [2, 8]. Different techniques for improving the formation of SAPO-34 nanocrystals have been developed [9-12], but recently there has been a rapid increase in the application of unconventional methods [13, 14]. Sonochemical synthesis by US irradiation (20 kHz–10 MHz [15]) is a new method for synthesis of nanoparticles especially nanocatalysis. Contrary to conventional methods (mainly hydrothermal synthesis), this method is very simple, fast, and does not need any complicated facilities. In this method, the size of particles can be easily controlled by changing the ultrasound-related variables. Chemical effects of US waves are due to acoustic cavitation phenomena in the solution. Due to the collapse of bubbles, a temperature and pressure of about 5,000–25,000 K and 181.8 MPa [15] are produced. Collapsing of bubbles occurred in less than a nanosecond and so, a high rate of temperature decrease (10^{11} K/s) takes place, which prevents the organization and agglomeration of particles [6, 7].

A lot of parameters affect the sonochemical synthesis and its products. Some of these effecting parameters are: frequency and power of US waves, time of irradiation, solution temperature, type of solution, reaction vessel diameter, the kind of noble gas used in the reaction environment and even geometrical characteristics of the US device (e.g. horn type size) [16–19].The US typically used in common crystallization media (mainly aqueous media) falls in the low-frequency range (namely, 15, 20, 25 and 30 kHz) [20].

There are many references use Evolutionary Algorithm (EA) techniques in chemistry and catalysis includes Genetic Algorithm (GA), Evolutionary Strategy (ES), Genetic programming (GP), etc.

Evolutionary Strategy (ES) is used for selection and optimization of heterogeneous catalytic materials [21, 22]. Genetic Programming has been employed very few. Baumes et al. [23, 24] showed two examples of this very powerful technique. Genetic Algorithms (GA) have been done by various groups such as Pereira el al. [25] study. They reported a study of the effect of Genetic Algorithm (GA) configurations on the performance of heterogeneous catalyst optimization. Also, Gobin et al. [26, 27] used multi-objective experimental design of experiments based on a genetic algorithm to optimize the combinations and concentrations of solid catalyst systems. Moreover, genetic algorithm merges with knowledge based system [28] and has been boosted on a GPU hardware to solve a zeolite structure [29, 30]. In addition, GA has been used for crystallography and XRD measurements [31, 32] and as an Active Learning method for effective sampling [33].

2. Problem statement and objectives of the present study

Recently, we prepared SAPO-34 nanocrystals with a crystal size of about 50 nm by means of an efficient US procedure [34] and effects of ultrasound-related variables on sonochemical synthesis of SAPO-34 nanocrystals were investigated [19]. The physicochemical characteristics of SAPO-34 catalysts, i.e. crystallinity, BET surface area, crystal size and shape are controlled by adjusting US power intensity, sonotrode size, US irradiation time and sonication temperature. In this study, first, the catalytic performance of the SAPO-34 nanocrystals synthesized sonochemically under various US conditions (US power intensity, sonication temperature, irradiation time and sonotorode size) in MTO reactions are studied. Afterwards, an artificial neural network and MLR model is applied for the prediction of catalytic performance. Finally, optimization of the catalytic performance is considered using the hybrid of NSGA-II based ANN. The ANN is used as a fitness evaluation inside the NSGA-II. The main objectives of optimization were maximum conversion of methanol, maximum light olefins content and maximum lifetime.

3. Experimental

3.1. Catalyst preparation and characterization

The SAPO-34 catalysts were synthesized by the sonochemical method as described elsewhere [19, 34] using precursor gel with molar ratio of $1.0Al_2O_3$: $1.0P_2O_5$: $0.6SiO_2$: 2.0 TEAOH: $70H_2O$. The sources for Al and P were Aluminum isopropoxide [98% Al $(OPr^i)_3$, Merck] and H_3PO_4 [85 wt. % aqueous solution, Merck], respectively. Tetraethylammonium hydroxide [TEAOH, 20 wt %, Aldrich] was used as structure directing agent (SDA). Tetraethylorthosilicate [TEOS, Merck] was chosen as silica source for preparing primary gels. Aluminum isopropoxide was initially mixed with template (TEAOH) and deionized water at room temperature and stirred for an hour. Silica source (TEOS) was then added and stirred. Finally, with continuous stirring, phosphoric acid was added dropwise to the above solution.

The initial gel was irradiated with US waves at a frequency of 24 kHz. US irradiation was accomplished by means of US Processor UP200H (Hielscher) using titanium sonotrodes having tip diameters of 3, 7 and 14 mm with different US power intensities. The amount of initial gel used for the sonication is 50 ml in each run .The sonication temperature was controlled at a temperature of 20, 30, 40 and 50°C. The duration of irradiation was from 5 to 30 min. After insonation, the initial gel was placed in a 30ml Teflon-lined stainless steel autoclave and heated in an oven at 200 ºC for 1.5 h. The synthesis conditions of samples are given in Table 1.

The solid product was recovered and washed three times by centrifuging with distilled water, and then dried at 110 ºC. The as-synthesized crystals were calcined at 560 ºC in air for 5h to remove the organic template molecules. Powder X-ray diffraction (XRD) patterns were recorded in step scanning on a Philips PW3050 X-ray diffractometer by using CuKα radiation (λ =1.54 ºA) operating at 40 kV and 40 mA. The phase purity and the overall crystallinity were appointed by XRD. Crystallinity characterization of the samples was calculated by the following equation:

$$\text{Crystallinity} = \frac{\sum I}{\sum I_r} \times 100$$

where I is the line intensity of the sample and Ir is the line intensity of the reference sample, using the product having the highest crystallinity, as identified by XRD. The line intensities of the XRD pattern at 2h equal to 9.5 and 20.5 were employed for these calculations. The crystal morphology was analyzed by scanning electron microscopy (SEM, Philips XL30). The mean crystal diameters of the SAPO-34 samples were estimated by measuring the particle size of 100 particles on SEM images using Microstructure Measurement software. From the results, the mean crystal size was calculated as d, by the formula mentioned below [19]:

$$d = \frac{\sum n_i d_i^3}{\sum n_i d_i^2} \qquad (1)$$

d is a measure of volume/outer surface (d_i= size of particles)**.** The BET surface areas of calcined samples were determined from isotherm data of nitrogen adsorption data in the relative pressure (P/P_0) range of 0.05–0.30 obtained at 77.35 K using a Quantachrome Autosorb-1 analyzer. The surface acidity of the catalysts was measured by temperature programmed desorption of ammonia (NH_3-TPD) using a Micrometrics TPD/TPR 2900 analyzer with a TCD detector. The amount of ammonia desorbed from the catalyst was measured by comparing the TPD areas with that for the standard sample.

3.2. Catalytic performance

The conversion reactions of MTO over SAPO-34 catalysts were carried out in a fixed bed reactor made of quartz glass (id. 15mm) with a continuous-flow system containing a preheater and a catalyst bed under atmospheric pressure. The catalyst (0.6 g) charged in the catalyst bed at the center of the quartz reactor was activated at 500 °C in a nitrogen flow of 100 ml/min for 1 h before starting each reaction run and then cooled to the reaction temperature of 450 °C. A liquid mixture of methanol in water (20 vol %) was fed into the reactor. The feed rate was adjusted to 0.29 ml/min. The weight hourly space velocity (WHSV) was 4.5 h^{-1}. In the preheating zone (upper part of the reactor), the temperature increased to 450 °C in atmospheric pressure and the feed evaporates. In the catalyst bed at the center of the reactor, methanol vapor converted to light olefins.

The analysis of the reaction products was performed using an on-line gas chromatograph Agilent GC (6890 N), equipped with a flame ionization detector (FID) and Plot-Q column. Methanol conversion (X_{CH3OH}) and light olefins content ($C_2H_4 - C_3H_6$) are defined as below:

$$X_{CH_3OH} = \frac{mass\ of\ CH_3OH\ fed - mass\ of\ CH_3OH\ unreacted}{mass\ of\ CH_3OH\ fed} \quad (2)$$

$$Light\ Olefins\ (wt\%) = \frac{mass\ of\ ethylene\ and\ propylene}{mass\ of\ all\ hydrocarbon\ products\ including\ DME} \times 100 \quad (3)$$

3.3. ANN modeling

ANNs are widely accepted as an information processing methodology inspired by the working process of the human brain. ANNs are efficient in handling the nonlinear relationship in data [35]. The empirical models and correlations developed by conventional methods such as different types of multiple regression are complex in nature, difficult to predict non-linear relationships, less accurate, and require long computing time. The ANN has numerous advantages, including accurate approximations of complex problems, greater efficiency than traditional statistical-based prediction models such as regression even for multiple response computations, and greater effectiveness even with incomplete and noisy input data [36].

ANN constitutes a branch of artificial intelligence which has recently undergone rapid evolution and progress [37]. ANN acts as a black box model, which is composed of interconnected processing units called artificial neurons or nodes [35]. The ANN approach has the ability to learn highly non-linear relationships and processes information by its dynamic system response to external inputs [36].

There are several types of ANNs such as multilayer feed forward neural network (FFNN), recurrent, radial basis, function networks and self-organizing maps. The universal approximation theorem for neural networks states that every continuous function that maps intervals of real numbers to some output interval of real numbers can be approximated arbitrarily closely by a multi-layer perceptron with just one hidden layer. This result holds for a wide range of activation functions, e.g. for the sigmoidal functions. So in this study, a multilayer feed forward neural network is used. The multilayer feed forward neural network consists of an input layer, one or more hidden layers and an output layer [35, 38]. In this study, the input layer is composed of 3 nodes, which are the US intensity, US irradiation time and sonication temperature. The output layer has three nodes, which are maximum conversion of methanol, maximum light olefins content and nanocatalyst life time which is time on stream where methanol conversion is more than 73%. There is no general rule for the determination of the optimum number of nodes in the hidden layer and usually it is determined through trial and error [35, 38-40].

The nodes between each layer are connected with adaptable weights. The general working principle of the artificial neuron or node can be demonstrated as [35]:

$$y_i = f\left(\sum_{j=1}^{n} x_j w_{ij} + b_i\right) \tag{4}$$

where, x_j is the input from the previous node j, w_{ij} is the weight that connects node i and node j, n is the total number of previous nodes connecting with node i, b_i is bias of node i and f is activation (transfer) function. Feed forward neural networks with one hidden layer can approximate virtually any linear or nonlinear function to an acceptable accuracy, if sufficient hidden layer nodes are provided with the sigmoid function as the hidden layer activation function and the linear function as the output layer activation function [35]. In this study, the tansig function and the purelin function are used as the activation functions in the hidden layer and the output layer, respectively. Therefore, a feed forward neural network with one hidden layer is applied to predict the experimental data in this study.

Before using an artificial neural network, it is necessary to train the network. There are different kinds of training methods, in which back propagation is a common method [37]. In the current study, the back-propagation structure is implemented using different learning rules in the neural network approach.

Before using any method for training, an ANN has to normalize input and output. So input and output data are normalized between -1 and 1 by the following equation:

$$Normalize\ value = \frac{2[(Actual)_{value} - (minimum)_{Actual\ value}]}{(maximum)_{Actual\ value} - (minimum)_{Actual\ value}} - 1 \tag{5}$$

The prediction performance of the network is assessed by using statistical coefficients, i.e. root mean square error (RMSE), mean square error (MSE), correlation coefficient (R^2) and mean relative error (MRE) values [37, 40]. In this study, mean square error (MSE) and correlation coefficient (R^2) which are calculated by the following expressions are used as the correlation performance indicators of the network:

$$MSE = \frac{1}{n}\sum_{i=1}^{n}\left(y_{Actual(i)} - y_{calculated(i)}\right)^2 \quad (6)$$

$$R^2 = \frac{\left[\sum_{i=1}^{n}\left(y_{Actual(i)} - \bar{y}_{Actual}\right)\left(y_{Calculated(i)} - \bar{y}_{Calculated}\right)\right]^2}{\sum_{i=1}^{n}\left(y_{Actual(i)} - \bar{y}_{Actual}\right)^2 \sum_{i=1}^{n}\left(y_{Calculated\,(i)} - \bar{y}_{Calculated}\right)^2} \quad (7)$$

where $\bar{y}_{Actual}$ and $\bar{y}_{Calculated}$ are arithmetic means of actual and calculated values, respectively.

3.4. NSGA-II main process

The genetic algorithm is an optimization tool based on Darwinian evolution [41-43]. The principles, on which the NSGA-II relies, are the same as those of the single-objective optimization. The strongest individuals (or chromosomes) are combined to create the offspring by crossover and mutation and this scheme is repeated over many generations. However, the multi-objective optimization algorithm must consider the fact that there are many ‘‘best solutions”, which modify the selection process. NSGA-II sorts individuals based on the non-domination rank and the crowding distance to ensure a high level of performance as well as good dispersion of results [44-48]. In this study, the ANN was used as a fitness evaluation inside the NSGA-II. The flowchart of the hybrid of non-dominated sorting genetic algorithm-II based artificial neural networks (NSGA-II – ANN) program is shown in Fig. 1.

4. Results and discussion

4.1. Catalytic performance of SAPO-34 nanocatalysts

The methanol conversion and light olefins content (wt %) (C2=-C3=)over SAPO-34 catalysts synthesized by using the sonotrode having tip diameter of 7mm with different US power intensities are presented in Fig. 2. As indicated in Fig. 2, all SAPO-34 catalysts suffer activation in the first minutes of the process. The incomplete conversion of methanol in the early time on stream is due to the existence of an induction period [49] which can be explained by the hydrocarbon pool (HP) mechanism. Haw suggested that the MTO reaction proceeds by a HP mechanism with cyclic organic species such as Hexamethylbenzene (HMB) as reaction centers for light olefins production [49, 50]. The time for the formation of these cyclic organic species causes the induction period, i.e. an increase in activity before maximum conversion. Except for sample S1, all catalysts show a high conversion for a long time especially catalyst S4 which maintains its activity for 540 min. The S1 catalyst just shows a maximum

conversion of 81% after 60 min. A rapid fall for conversion is subsequently observed and it reaches 12% after 420 min.

The nano-sized catalyst S4 shows a high content (wt %) toward light olefins (ethylene and propylene) for 180 min (Fig. 2) and the light olefins content decreases afterwards. Even after the reaction time of 540 min the light olefins content can remain at 10% over S4. The decrease in light olefins formation corresponds to an increase in the formation of DME which can be explained by the catalyst deactivation [51]. At this reaction time, DME is the main product (79 wt %) and other products are butene and the alkanes (C1–C5 alkanes) mainly methane.

The catalysts S2 and S3 also show the same trend for light olefin but with lower amounts compared to the catalyst S4. In comparison, the content of light olefins over the SAPO-34 catalysts S1 is much lower than the others and it decreases rapidly (Supplementary information, Table I).

These catalytic behaviors can be explained by the differences in catalysts physicochemical properties which are affected by US power intensity. According to the results obtained previously [19], the crystallinity changes markedly with US power intensity and higher crystallinity is obtained with increasing US intensity. Therefore, the catalyst S1 synthesized at the lowest power intensity has the lowest crystallinity as shown in Table 1. Increasing the crystallinity results in the formation of more structural pores and it may enhance the diffusion rate and quantity of reactants into structure channels in crystallites [19]. Also, different US power intensities applied in the synthesis of SAPO-34 crystals alter the morphology and agglomeration of the products. It is clearly seen in Table 1 that with an increase in the US intensity the average crystal size of SAPO-34 crystals gradually decreases, as well as formation of uniform spherical nanocrystals (Supplementary information, Fig. I)instead of spherical aggregates of cube type SAPO-34 crystals seen previously [19]. By comparing the acidity of the SAPO-34 catalysts represented in Table 1, S2 and S1 samples have the highest and lowest concentration of strong acid site respectively, which could be active for MTO conversion, though the strength of their acid sites are similar. Therefore, the short lifetime of the catalyst S1 cannot be related to the strength and amount of acid sites but can be correlated with the crystallinity and crystal sizes of the catalyst. For larger crystals of the catalyst S1, the residence time in a crystal for the hydrocarbons is long because of the longer diffusion length. Saturated hydrocarbons and/or aromatic compounds cannot escape from the pores of SAPO-34, and successive polymerizations readily occur because of the long reaction time [2]. Therefore, the catalyst S4 possessing the higher crystallinity, smaller size and better dispersion [19] has less diffusion limitation and a longer lifetime[51]. Additionally, the formation of coke is inhibited over the smaller crystals of catalyst S4 as a result of the reduced resistance to diffusion, resulting in a much greater production of light olefins for longer reaction times.

Effects of the sonotrode size on the catalytic properties of SAPO-34 catalysts S4-S6 are shown in Fig.3. The catalyst S4 and S6 synthesized using the sonotrodes having tip diameters of 7, and 14 mm show a much higher conversion of methanol and maintain it for a longer time as well as a higher content toward light olefins compared to that synthesized with the sonotrode having tip diameters of 3 mm (S5). This can be explained by an increase in US power with increasing sonotrode size from 3 to 14 mm. Although the smallest sonotrode possesses the highest US intensity, i.e. 460 $W.cm^{-2}$ (related to 100% amplitude setting) compared to 300 and 105 $W.cm^{-2}$ (max intensities of sonotrodes having tip diameters of 7 and 14 mm, respectively), it has the smallest horn tip area, resulting in lower emitted US power. The increase in the US power results in the higher turbulence of the mixture and the satisfactory mixing can be achieved much more rapidly. The difference in US power results in different catalyst activities which can be attributed to the difference in the crystallinity and thus BET surface area of catalysts. It is clear from Table 1 that by increasing US power the crystallinity of samples increase (Supplementary information, Fig. II), resulting in the rise of BET surface areas.

Fig. 4 shows the role of US irradiation time on the methanol conversion and light olefin production. The catalyst irradiated for 5 min (S7) shows the lowest methanol conversion and the lowest olefin content on account of the absence of the crystal phase. At short times, the US wave fails to blend the solution uniformly and only a few nuclei are formed. Some small crystal particles cannot grow further due to the shorter US time. Applying US for longer times produces more apparent crystals and no large crystals can grow, because more nuclei will occur continuously until the level of super-saturation becomes very low [19,20]. With the extension of US irradiation time from 5 to 15 min, the methanol conversion as well as the olefin content increases sharply, and the samples irradiated for 15 and 30 min show the highest olefin selectivity. This result confirms that the activity of SAPO-34 samples improves with the rise in crystallinity.

Fig. 5 shows the catalytic performance of the products synthesized under different sonication temperatures of 20, 30, 40 and 50°C. With increasing the sonication temperature, the crystallinity of SAPO-34 products increases, smaller crystals with uniform size distribution are formed and the morphology of the product alters from cubic crystals to uniform nanocrystals since the temperature can affect the cavitation threshold. Generally, the cavitation threshold limit has been found to decrease with an increase in temperature. This means that cavitation bubbles are more easily produced as the temperature is raised. Therefore, higher sonication temperature leads to fast nucleation, which results in smaller particles in comparison to the lower sonication temperature [19]. According to Table 1, the catalysts S9 and S10 have the lowest amount of strong acid site concentration at 440–460°C and it falls in a narrow interval for samples S9 and S10, i.e., 0.69 and 0.60 respectively. Also, the acid strength of all

the samples is almost the same. Therefore, it can be concluded that the differences between the catalytic behaviors of samples could be more related to the crystal size and crystallinity of the catalyst.

4.2. ANN results

In this study, the multilayer feed forward neural networks with back-propagation structure are implemented using different learning rules in the neural network approach such as Bayesian regulation (BR), Levenberg-Marquardt (LM), Scaled conjugated gradient (SCG) and RPROP back propagation (RP). In the Bayesian regulation rule, the input data are divided into two parts; 70% and 30% of the data are used for training and test, respectively, but in other learning rules the input data are divided into three parts; 70%, 15% and 15% of the data are used for training, validation and test, respectively. The values of the training and test data are normalized between -1 and 1 by using Eq. (5). The number of data used in the network is 54. In this data set the sonotrode size is 7mm. The range of all experimental conditions used for modeling with ANN is shown in Table 2.

The results of the network models for different neuron numbers in the hidden layer using different training algorithms are presented in Table 3. The correlation performance of the network is assessed by using mean square error (MSE) and correlation coefficient (R^2) values. It can be seen that the Bayesian regulation back propagation algorithm with 10 neurons in the hidden layer is the best training procedure that achieved the highest R^2 and lowest MSE. Thus, the optimum number of neurons is used to create the network topologies which were 3–10–3. Here, the numbers in the expressions of the network topologies represent the neuron numbers in the input layer, the hidden layer and the output layer, respectively.

Fig. 6 explains comparison plots between network output and the corresponding experimental data of the catalytic performance of SAPO-34 nanocatalysts synthesized sonochemically, for training and test data using the BR training rule and 3-10-3 topology. This figure shows that there is a very good agreement between this ANN model and experimental values. The comparison between network predicted and experimental data can be seen in Table II of Supplementary information. Fig. 7 shows the performance graph. It is observed that the desired goal has been reached in 1000 epochs, and the ANN with ten hidden neurons could achieve the convergence. The errors of data attained by the optimum ANN model are plotted out versus the frequency of data in Fig. 8. A normal distribution of variation brings about a specific bell-shaped curve (Gaussian curve), with the highest point in the middle and smoothly curving symmetrical slopes on both sides of center. These figures illustrate an approximately normal distribution of errors produced by the model. The Gaussian curve reveals that our results are symmetrical [38].

The methanol conversion, light olefins content and catalyst life time are illustrated versus US power intensity, sonication temperature and irradiation time in supplementary information (Figs III to V in

supplementary information). Also a Matlab user-friendly code is given as supplementary data for verification of ANN results (‘ANN.m', 'deNormalize FCN.m' and 'Normalize FCN.m' in supplementary information).

The 3-fold cross-validation (3-CV) of model is used in this section because of the low number of points. The original sample is randomly partitioned into three equal size subsamples. Of the three subsamples, a single subsample is retained as the validation data for testing the model, and the remaining two subsamples are used as training data. The cross-validation process is then repeated three times (the folds), with each of the three subsamples used exactly once as the validation data. The three results from the folds are averaged to produce a single estimation. The results of the 3-CV models are presented in Table 4. This shows that this model is achieved the very high R^2 and low MSE. The advantage of this method is that all observations are used for both training and validation, and each observation is used for validation exactly once.

4.3. MLR model results

In this section, the traditional models of objection functions includes methanol conversion, light olefins content and catalyst life time, obtained through liner regression analysis, are presented. These models used US power intensity, sonication temperature and irradiation time point as input variables. These models are shown in Equations 7-9 and comparison plots between the model output and its corresponding experimental data are given in Fig. 9.

$$X_{CH_3OH} = 0.1082 \times P + 0.7721 \times t + 1.1298 \times T \quad (8)$$

$$LO = 0.0946 \times P + 0.5296 \times t + 0.9030 \times T - 0.9122 \quad (9)$$

$$\tau = 0.4919 \times P + 0.1942 \times t + 4.4912 \times T \quad (10)$$

Where X_{CH_3OH}, LO, τ, P, t and T are methanol conversion (%), light olefins content (wt%), life time (min), US power intensity (W/cm^2), sonication temperature ($^{\circ}C$) and irradiation time (min) respectively.

The results indicate a poor fit between experimental and predicted data with low coefficient of determination. Thus, the objective functions prediction of using these traditional models may not be reliable. Table 5 shows a comparison between ANN and MLR model results. This confirms the ANN technique is more effective in predicting the objective functions tested in this study than the traditional statistical-based prediction models.

4.4. Optimization results using NSGA-II

In this section, the hybrid NSGA-II based ANN is used to optimize catalytic performance of SAPO-34 nanocatalysts synthesized sonochemically in MTO reaction and obtains Pareto-optimal solutions. In other words, the ANN is used as a fitness evaluation inside the NSGA-II. A Pareto-optimal set is a series of solutions that are non-dominated with respect to each other. While moving from one Pareto solution to another, there is always a certain amount of sacrifice in one objective(s) to achieve a certain amount of gain in other(s).

The objectives of optimization were minimum unreacted methanol, maximum light olefins content and maximum life time. Thus, the objectives included:

Objective 1: Maximizing X_{CH_3OH} (11)

Objective 2: Maximizing light olefins content (wt %) (12)

Objective 3: Maximizing Life time (min) (13)

The constraints were:

$20^{\circ}C \leq$ Sonication Temperature $\leq 50^{\circ}C$ (14)

US Intensity= 12, 27, 48, 75, 108, 147, 192, 243, 300 $W.cm^{-2}$ (15)

$5\,\text{min} \leq$ US Irradiation time $\leq 30\,\text{min}$ (16)

The objective functions are optimized full filling the constraints given in Eqs. (14) – (16). The sonotrode size is 7mm. A population size of 100 is chosen with crossover probability of 0.7 and mutation probability of 0.1. Arithmetic crossover and gauss method were used as crossover and mutation methods, respectively.

The optimum solutions have been listed in Table 6. This table shows that each of the solutions is better than the other in at least one of the objective functions. Thus, the user has to decide on the ultrasound-related variables based on the ease of operation, experience, the cost involved and also the quality of the product (Fig. VI in supplementary files). . Three samples of optimum solutions are validated experimentally Table 7 shows a comparison between experimental and predicted values. The results indicate that there is an acceptable agreement between experimental and predicted results by NSGAII–ANN. The methanol conversion, light olefins content and catalyst life time of optimum solutions are illustrated versus US power intensity, sonication temperature and irradiation time in supplementary information (Figs VII to IX in supplementary information.)

Conclusion

MTO reaction was investigated over SAPO-34 nanocatalysts synthesized sonochemically under various US conditions. The sonochemically prepared catalysts were used to elucidate the effects of US power intensity, sonication temperature, irradiation time and sonotorode size on their catalytic performance, especially in terms of methanol conversion, light olefin content and catalyst lifetime. The catalysts synthesized with higher US power (adjusted by both the size of sonotrode or US power intensity) show a much higher conversion of methanol and maintain it for a long time as well as a high content toward light olefins. With increasing the sonication temperature and irradiation time, the methanol conversion as well as the light olefin content increases. Afterwards, the multilayer feed forward neural network with back-propagation structure was implemented using different learning rules in the neural network approach. The ANN with a 3-10-3 architecture and Bayesian regulation training rule has the best fit and was selected as the optimum ANN model for prediction. The tansig and purelin functions were used as the activation functions in the hidden and output layers, respectively. In the optimum model, the input data were divided into two parts; 70% and 30% of the data were used for training and test, respectively. The results indicate that there is a very good agreement between experimental and predicted results by ANN. Also, the multiple linear regressions (MLR) was used to predict these objective functions. The results indicate a poor fit for the objective functions with low coefficient of determination. This confirms the ANN technique is more effective than the traditional statistical-based prediction models. Finally, the hybrid NSGA-II based ANN was used and introduced the best catalytic performance of SAPO-34 nanocatalysts synthesized sonochemically under various US conditions in the MTO reaction and the ANN was used as a fitness evaluation inside the NSGA-II. . Such methodology (hybrid of ANN and NSGA-II) allowed the researchers to find a near optimum solution to their problem where multiple input and output variables are interacting. Despite the relative simplicity of the search space, human understanding and capture of the variables relationships still remains complicated. Therefore such approach shows how the use of both a modelling and an optimization strategy allow tackling this challenge.

Acknowledgements

The financial supports from the Iran National Science Foundation are gratefully acknowledged.

References

[1] S.M.A. Ahmadi, S. Askari, R. Halladj ,Afinidad. 562(3013)130

[2] Y. Hirota, K. Murata, M. Miyamoto, Y. Egashira, N. Nishiyama, Catal. Lett. 140(2010) 22

[3] S. Askari, Z. Sedighi, R. Halladj, Micropor. Mesopor. Mater. 197 (2014) 229

[4] N. Nishiyama, M. Kawaguchi, Y. Hirota, D.V. Vu, Y. Egashira, K. Ueyama, Appl. Catal. A: Gen (2009) 193–199

[5] B.P.C. Hereijgers, F. Bleken, M.H. Nilsen, S. Svelle, K. Lillerud, M. Bjørgen, B.M. Weckhuysen, U. Olsbye, J. Catal. 264 (2009) 77

[6] S. Askari, R. Halladj, B. Nasernejad, J. Mater. Sci-Poland. 27 (2009) 397

[7] J. Talebi, R. Halladj, S. Askari, J. Mater. Sci. 45 (2010) 3318

[8] D. Chen, K. Moljord, T. Fuglerud, A. Holmen, Micropor. Mesopor. Mater. 29 (1999) 191

[9] M. Razavian, R. Halladj, S. Askari, Rev. Adv. Mater. Sci. 29 (2011) 83

[10] B. Valizadeh, S. Askari, R. Halladj, A. Haghmoradi, Syn. React. Inorg. Metal. 44 (2014) 79

[11] N. Najafi, S. Askari, R. Halladj, Powder .Technol. 254 (2014) 324

[12] S. Askari, R. Halladj, M. Sohrabi, Rev. Adv. Mater. Sci. 32 (2012) 14

[13] F. Marzpour, S. Askari, R. Halladj, Rev. Chem. Eng. 29 (2013) 99

[14] F. Marzpour, R. Halladj, S. Askari, Powder. Technol. 221 (2012) 395

[15] A. Gedanken, Ultrason. Sonochem. 11 (2004) 47

[16] S. Askari, S. Miar Alipour, R. Halladj, M. H. Davood Abadi Farahani, J. Porous. Mater. 20 (2013) 285

[17] S. Askari, R. Halladj, M. Nazari, Mater. Res. Bull. 48 (2013) 1851

[18] B. Nanzai, K. Okitsu, N. Takenaka, H. Bandow, N. Tajima, Y. Maeda ,Ultrason. Sonochem .16(2009) 163

[19] S. Askari, R. Halladj, J. Solid. State. Chem. 201 (2013) 85

[20] H. Li, J. Wang, Y. Bao, Z. Guo, M. Zhang, J. Cryst. Growth. 247 (2003) 192

[21] F. Clerc, M. Lengliz, D. Farrusseng, C. Mirodatos, R.M. S.R.M. Pereira and R. Rakotomalala, Review of Scientific Instruments 76 (2005) 062208

[22] D. Wolf, O.V. Buyevskaya and M. Baerns, Applied Catalysis A: General, 200 (2000) 63

[23] L.A. Baumes, A. Blansché, P. Serna, A. Tchougang, N. Lachiche, P. Collet and A. Corma, Materials and Manufacturing Processes, 24 (2009) 282

[24] L.A. Baumes and P. Collet, Computational Materials Science, 45 (2009) 27

[25] S.R.M. Pereira, F. Clerc, D. Farrusseng, J.C. van der Waal, T. Maschmeyer and C. Mirodatos, QSAR & Combinatorial Science, 24 (2005) 45

[26] O.C. Gobin, A. Martinez Joaristi and F. Schüth, Journal of Catalysis, 252 (2007) 205

[27] O.C. Gobin and F. Schüth, Journal of Combinatorial Chemistry, 10 (2008) 835

[28] J. M. Serra, A. Corma, D. Farrusseng, L.A. Baumes, C. Mirodatos, C. Flego and C. Perego, Catalysis Today, 81 (2003) 425

[29] J. Jiang, J.L. Jorda, J. Yu, L.A. Baumes, E. Mugnaioli, J.M. Diaz-Cabanas, U Kolb and A. Corma, Science, 333 (2011) 1131.

[30] A. Rimmel, F. Teytaud and T. Cazenave, Optimization of the Nested Monte-Carlo Algorithm on the Traveling Salesman Problem with Time Windows, in Applications of Evolutionary Computation, G. Goos, J. Hartmanis and J.v. Leeuwen, Editors. 2010, Springer. p. 501-511.

[31] L.A. Baumes, M. Moliner and A. Corma, Chemistry – A European Journal, 2009, 15, 4258.

[32] L.A. Baumes, M. Moliner, N. Nicoloyannis and A. Corma, CrystEngComm, 2008, 10, 1321.

[33] L.A. Baumes, Journal of Combinatorial Chemistry, 2006, 8, 304.

[34] S. Askari, R. Halladj, Ultrason. Sonochem.19 (2012) 554–559

[35] X. Meng, M. Jia, T. Wang, Fuel. 121 (2014) 133-140

[36] L. Kamble, D. Pangavhane, T. Singh, Int. J. Heat. Mass. Tran. 70 (2014) 719-724

[37] A. Tardast, M. Rahimnejad, G. Najafpour, G. Ghoreyshi, G.C. Premier, G. Bakeri, S.E. Oh, Fuel. 117 (2014) 697-703

[38] R. Badrnezhad, B. Mirza, J. Ind. Eng. Chem. 20 (2014) 528-543

[39] A. Badday, A. Abdullah, K. Lee, Chem. Eng. Process. 75 (2014) 31-37

[40] Z. Tian, B. Gu, L. Yang, F. Liu, Appl. Thermal. Eng. 63 (2014) 459-467

[41] M.J. Azarhoosh, H. Ale Ebrahim, S.H. Pourtarah, Chem. Eng. Com. Doi: 10.1080/00986445.2014.942732

[42] M.J. Azarhoosh, F. Farivar, H. Ale Ebrahim, RSC. Adv. 4 (2014) 13419- 13429

[43] E.G. Shopova, N.G. Vaklieva-Bancheva, Comput. Chem. Eng. 30 (2006)1293-1309

[44] M. Bayat, Z. Dehghani, M.R. Rahimpour, J. Taiwan. Inst. Chem. E. 45(2014) 1474-1484

[45] M.M. Etghani, M.H. Shojaeefard, A. Khalkhali, M. Akbari, Appl. Thermal. Eng. 59 (2013) 309-315

[46] N. Agrawal, G.P. Rangaiah, A.K. Ray, S.K. Gupta, Chem. Eng. Sci. 62 (2007) 2346-2365

[47] A. Bakhshi Ani, H. Ale Ebrahim, M.J. Azarhoosh, Energy & fuels. DOI: 10.1021/acs.energyfuels.5b00467

[48] K. Deb, IEEE Trans. Evol. Comput.6 (2002) 182-197

[49] H. Hajfarajollah, S. Askari, R. Halladj, Reac. Kinet. Mech. Cat. 111(2014)723-736

[50] J.F. Haw, W.G. Song, D.M. Marcus, J.B. Nicholas. Acc. Chem. Res 36 (2003) 317-326

[51] S. Askari, R. Halladj, M. Sohrabi, Micropor. Mesopor. Mater. 163 (2012) 334-342

Figure captions:

Fig. 1. Flowchart of the NSGA-II – ANN program

Fig. 2. Methanol conversion and light olefins content (C_2H_4 – C_3H_6) over SAPO-34 catalysts synthesized with different ultrasound power intensities; S1:48 $W.cm^{-2}$, S2:108 $W.cm^{-2}$, S3:192 $W.cm^{-2}$, S4: 300 $W.cm^{-2}$.

Fig. 3. Effects of the sonotrode size on the catalytic properties of SAPO-34 catalysts; (S5):3mm, (S4):7mm, (S6):14mm.

Fig. 4. Effects of ultrasonic irradiation time on the methanol conversion and light olefin production over SAPO-34 catalysts; S7:5 min, S4:15 min, S8:30min.

Fig. 5. Catalytic performance of the SAPO-34 products synthesized under different sonication temperature; S9:20°C, S10:30°C, S11:40°C, S4:50°C.

Fig. 6. Comparison between experimental & ANN values (a) methanol conversion (%) (b) Light olefins content (wt %) (c) Lifetime.

Fig. 7. Performance graph

Fig. 8. Error histogram

Fig. 9. Comparison between experimental & MLR model values (a) methanol conversion (%) (b) Light olefins content (wt %) (c) Lifetime.

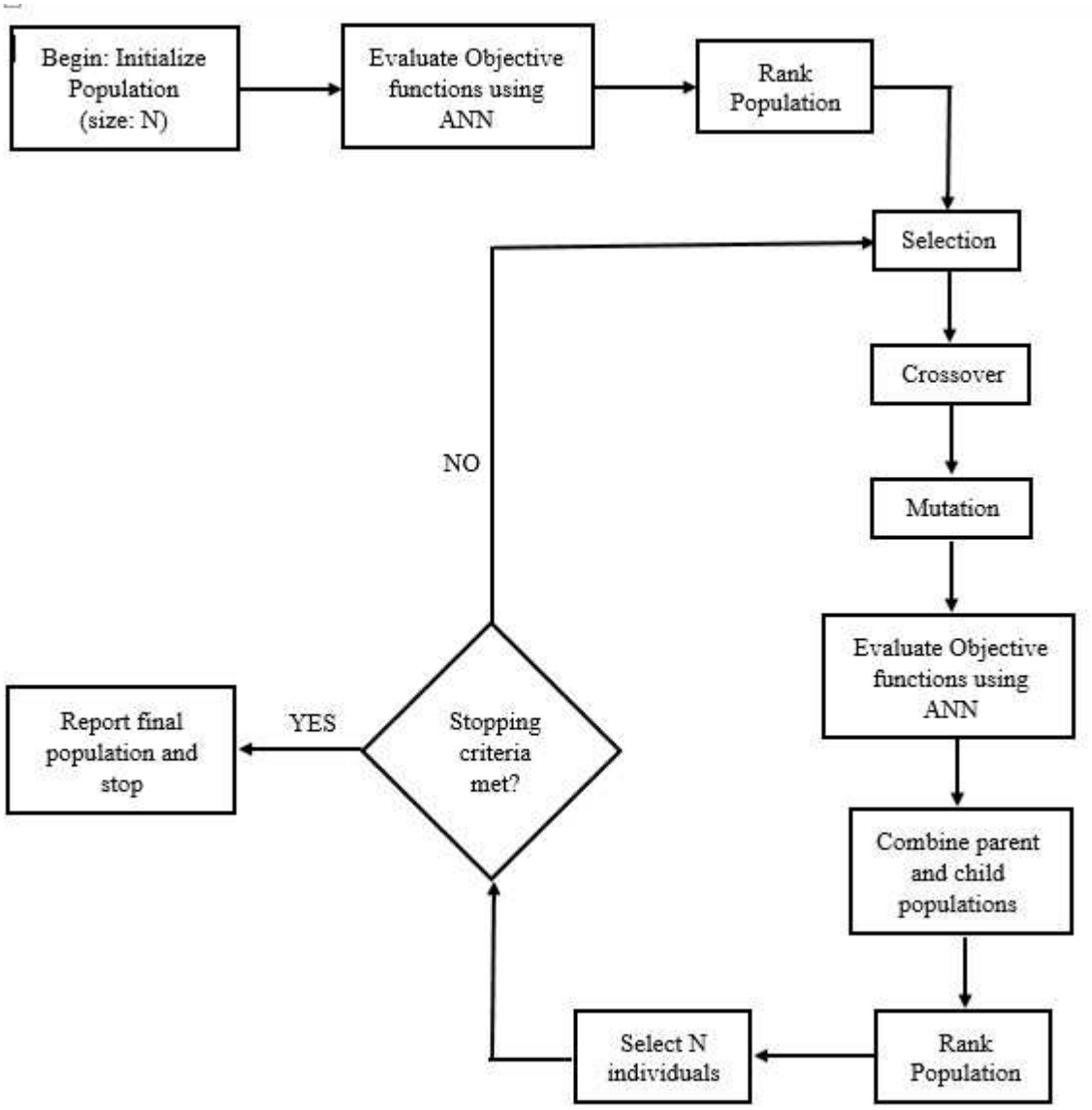

Fig. 1.

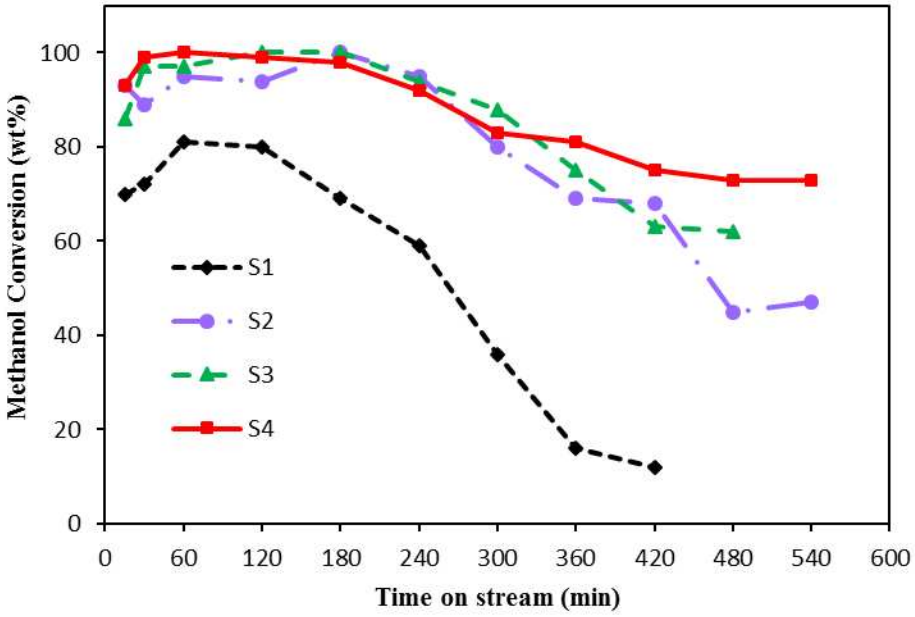

(a)

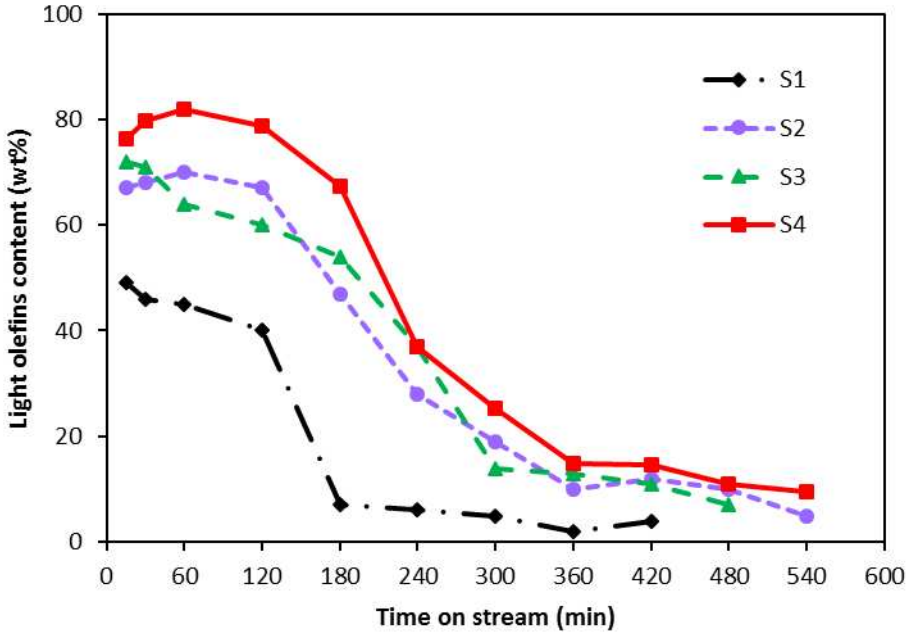

(b)

Fig. 2.

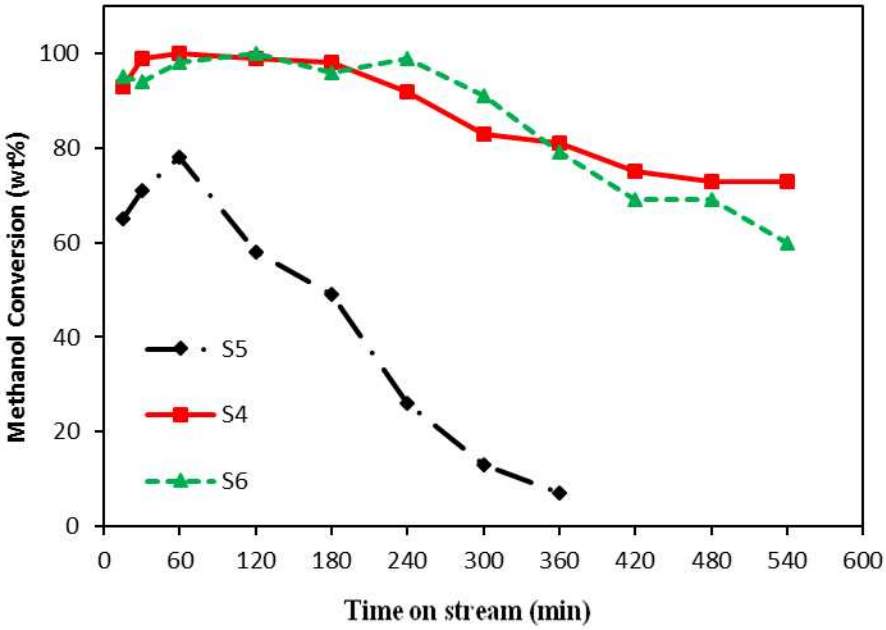

(a)

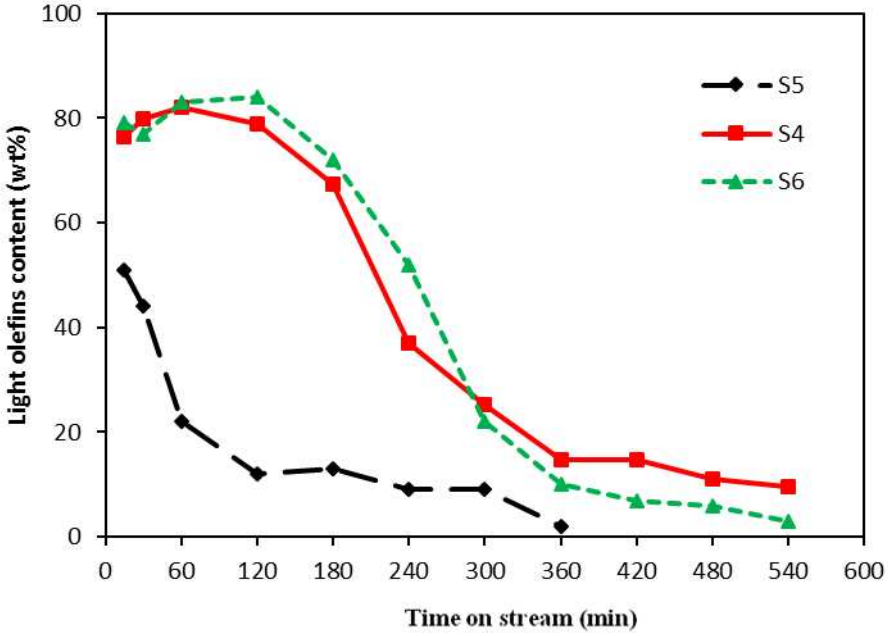

(b)

Fig. 3.

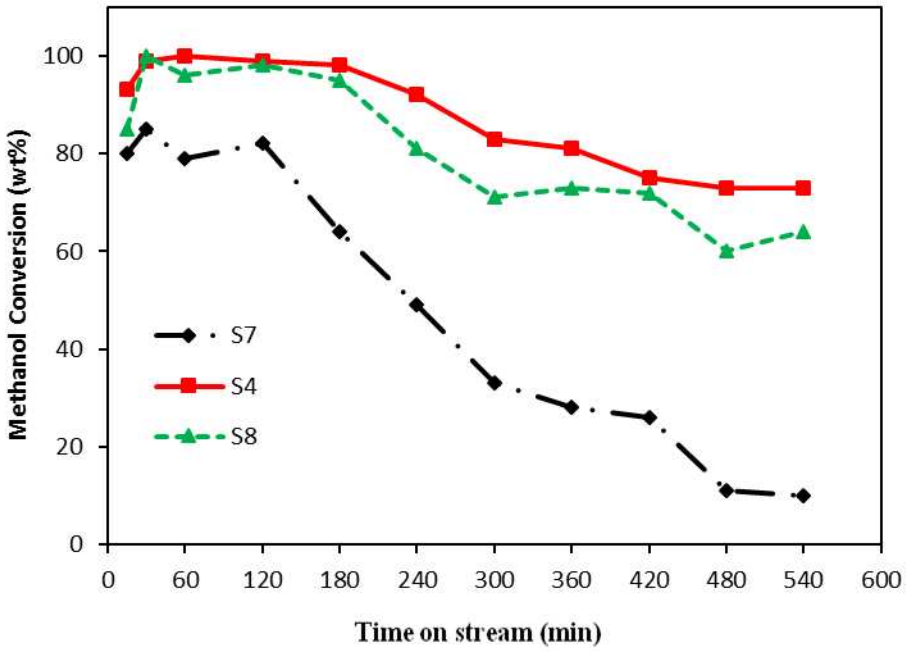

(a)

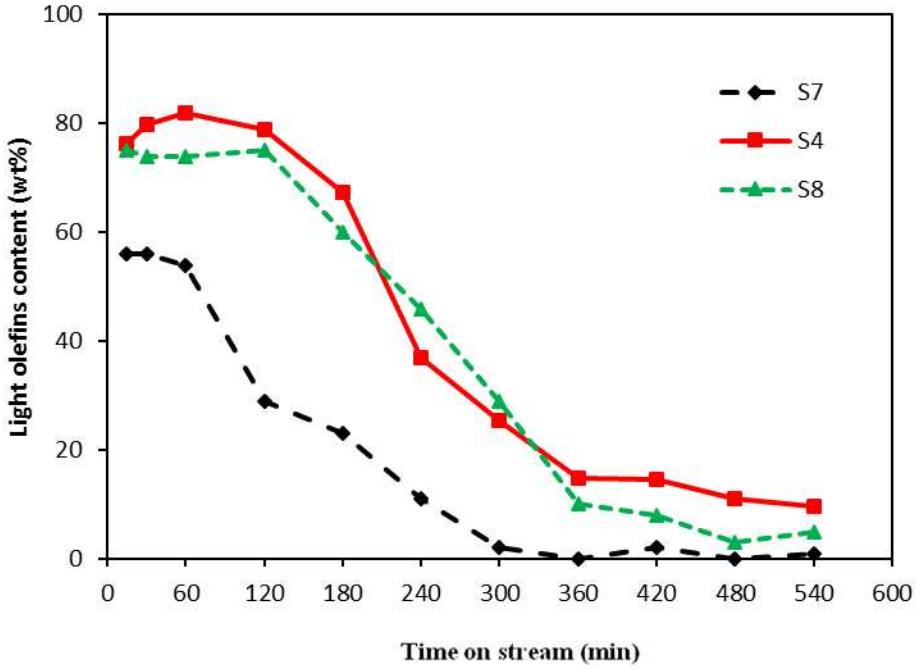

(b)

Fig. 4.

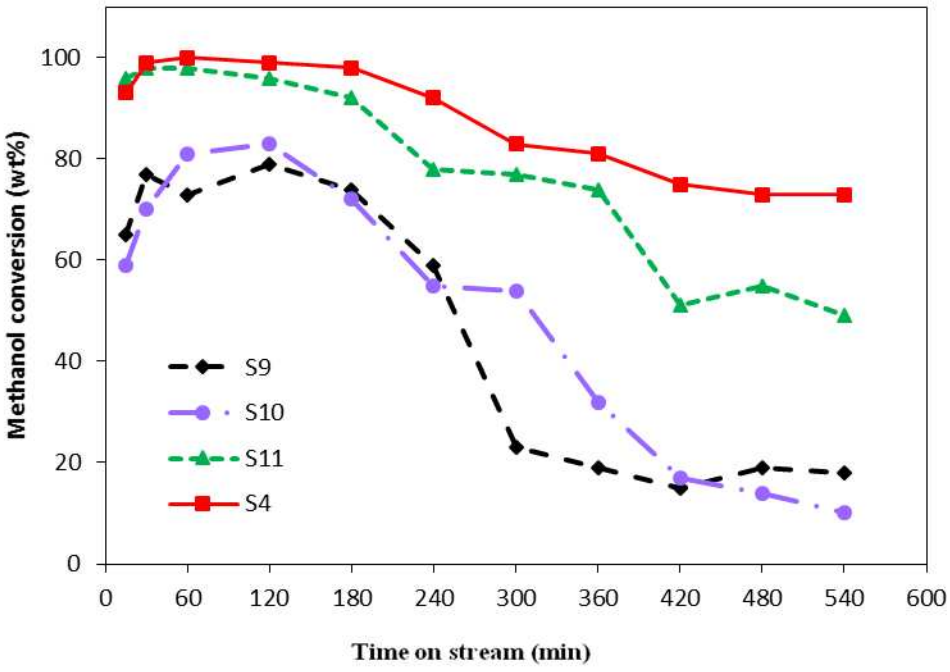

(a)

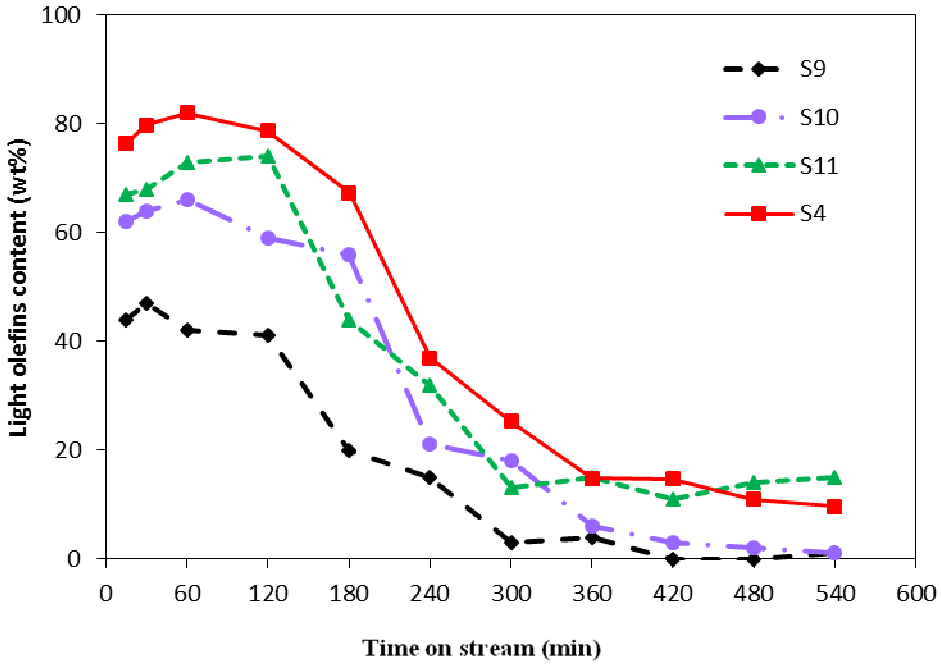

(b)

Fig. 5.

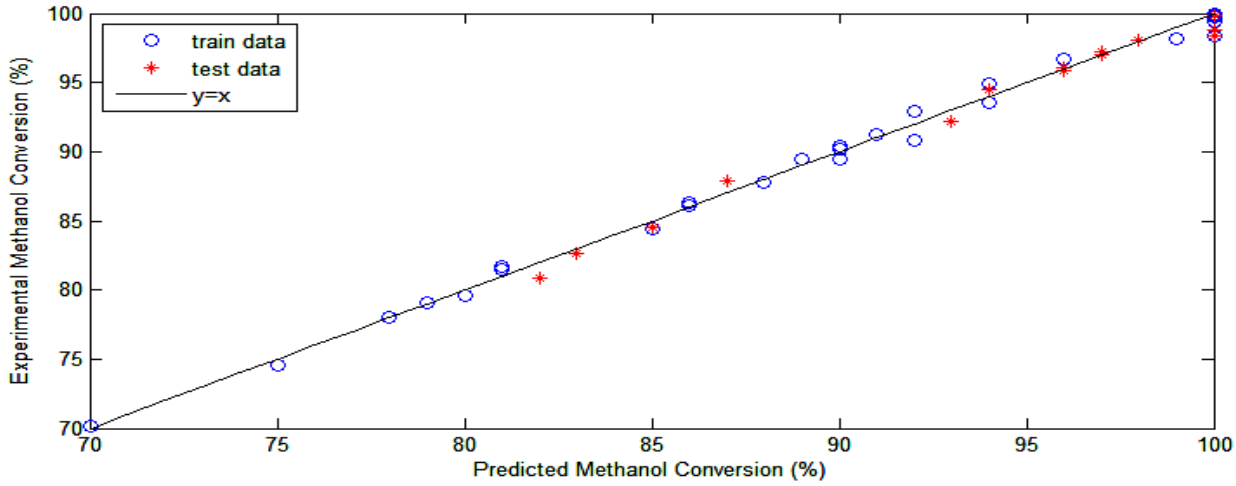

(a)

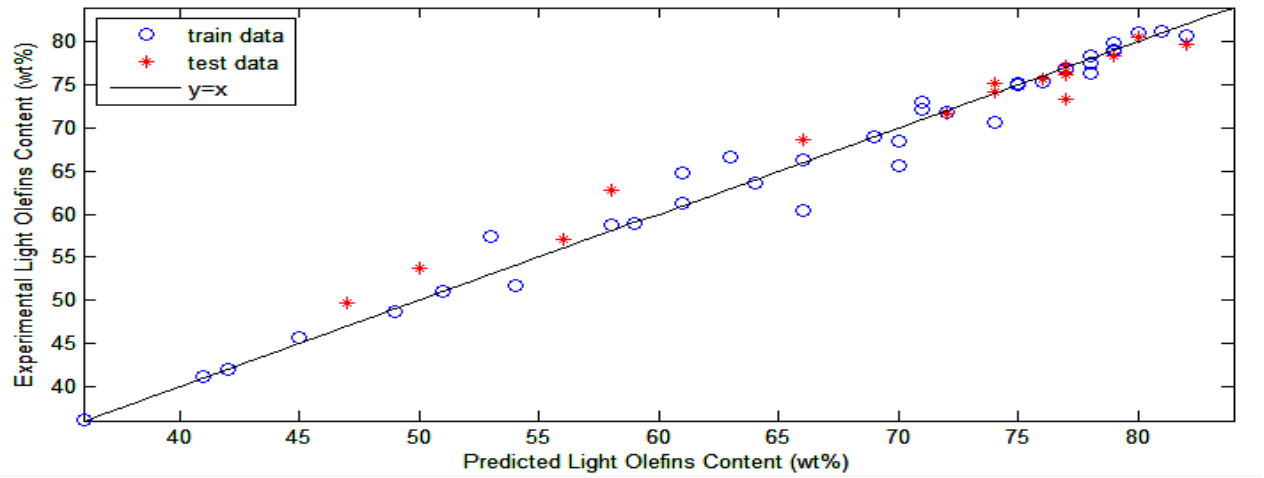

(b)

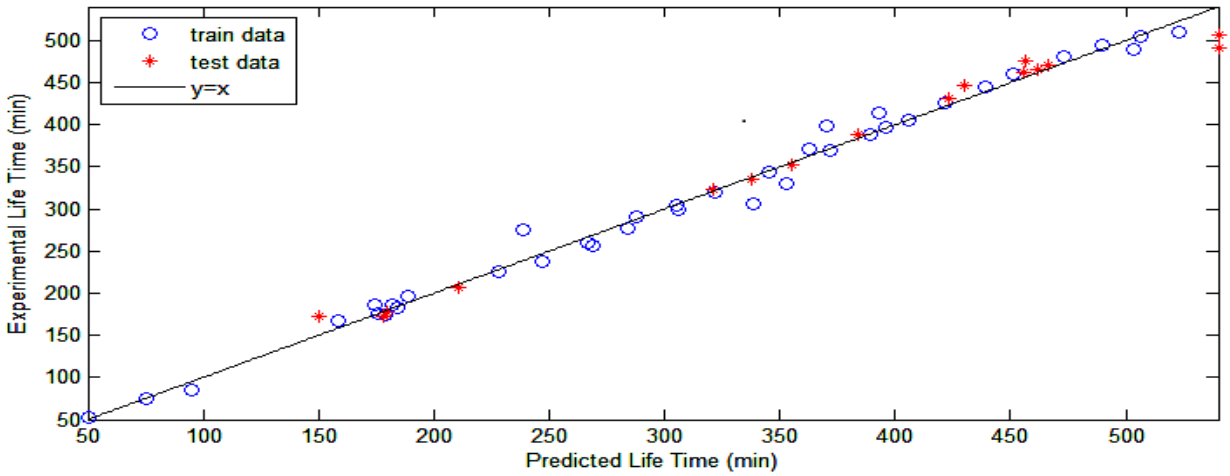

(c)

Fig. 6.

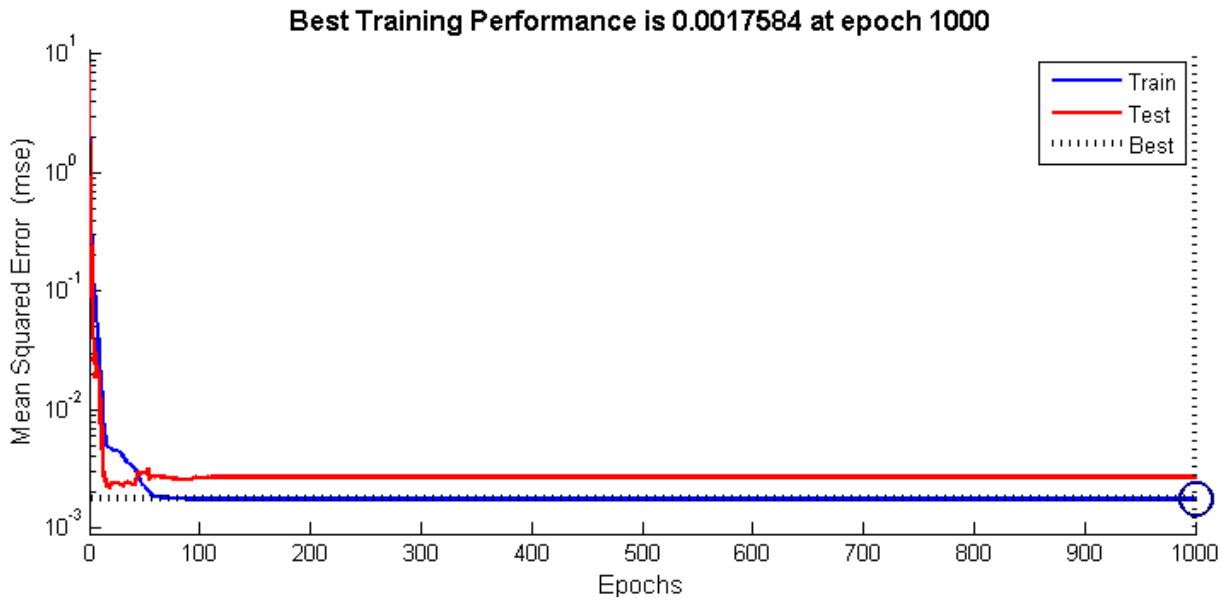

Fig. 7.

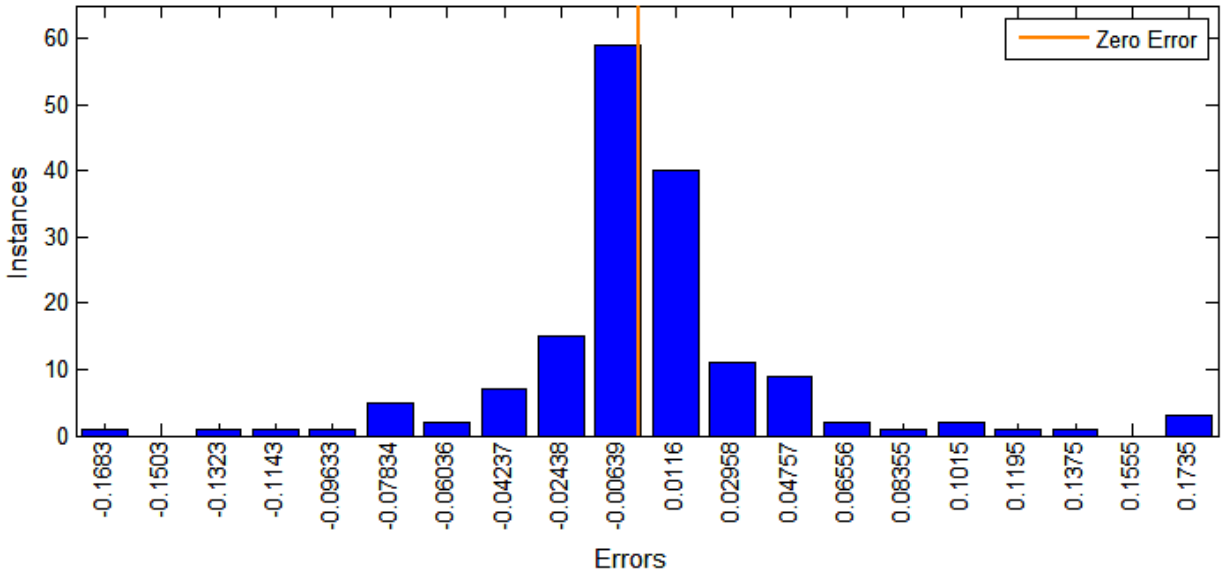

Fig. 8.

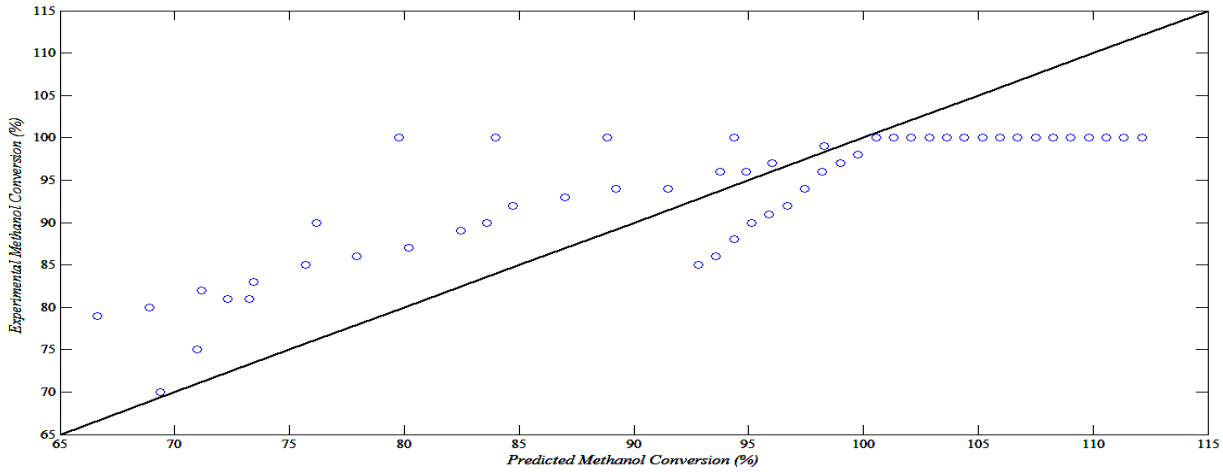

(a)

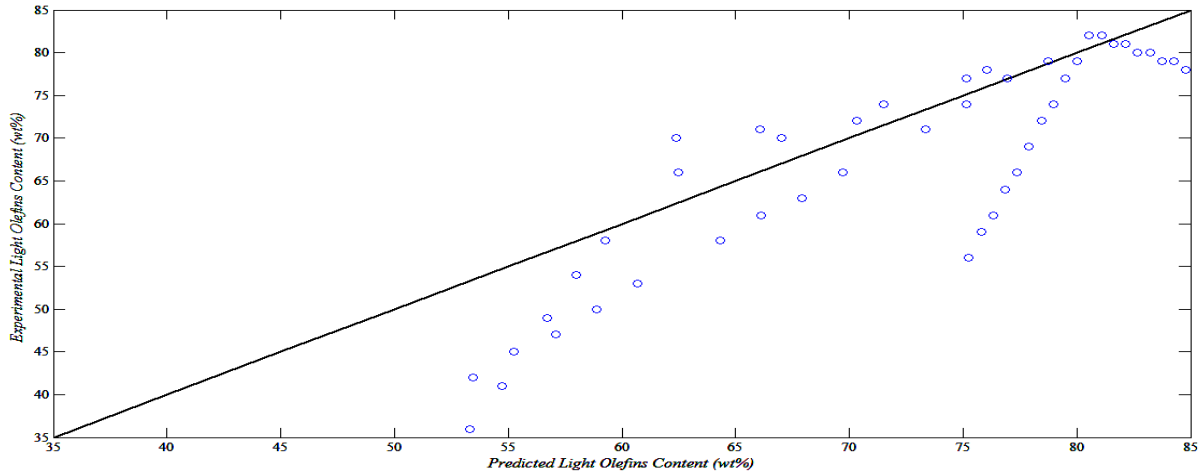

(b)

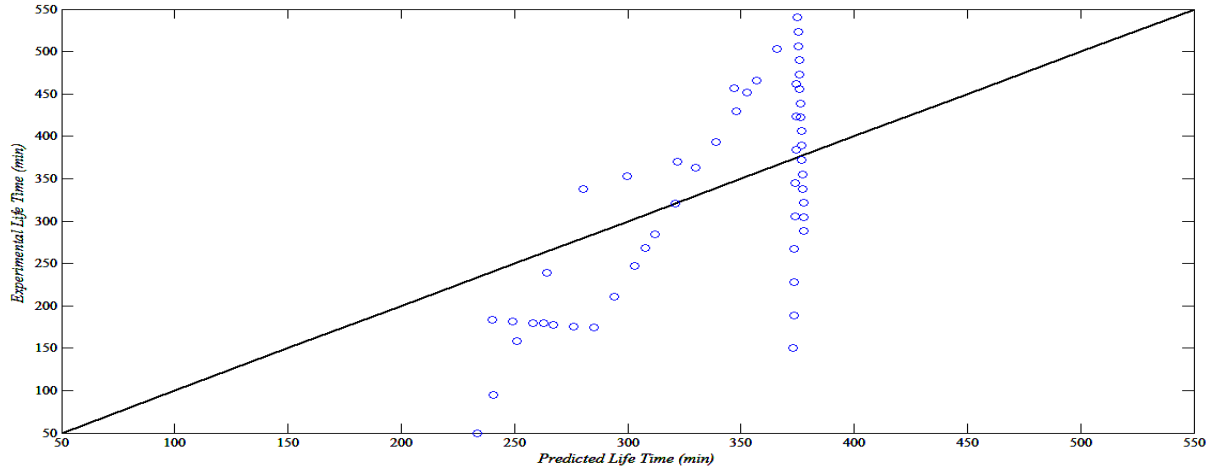

(c)

Fig. 9.

Tables:

Table 1. Sonochemical synthesis conditions and properties of the catalysts.

Table 2.Range of all experimental conditions used for modeling with ANN.

Table 3.Performance of different ANN methods for the prediction of catalytic performance of the SAPO-34 products synthesized in MTO reaction.

Table 4. The results of the 3-CV models

Table 5. Comparison between optimum ANN & MLR model results

Table 6.Pareto-optimal solution set after 200 generations.

Table 7. Comparison between experimental & predicted values of optimum solutions

Table 1

Sample	Ultrasonic power intensity ($W.cm^{-2}$)	Ultrasonic irradiation time (min)	Sonication temperature (°C)	Sonotrode diameter (mm)	Relative crystallinity (%)	Distribution of acid sites (mmol NH_3/g)		Mean crystal diameter (nm)	BET Surface area (m^2g^{-1})
						Weak 220-240°C	Strong 440–460 °C		
S1	48	15	50	7	40	0.86	0.71	150	329
S2	108	15	50	7	48	0.8	0.94	100	369
S3	192	15	50	7	68	0.74	0.79	70	392
S4	300	15	50	7	77	1.01	0.78	50	493
S5	460	15	50	3	38	0.9	0.73	135	306
S6	105	15	50	14	100	-	- Nd	66	444
S7	300	5	50	7	35	0.82	0.78	105	- Nd
S8	300	30	50	7	88	-	- Nd	58	429
S9	300	15	20	7	52	0.97	0.69	120	- Nd
S10	300	15	30	7	47	0.94	0.60	115	- Nd
S11	300	15	40	7	71	1.08	0.89	79	388

Nd: Not determined

Table 2

Inputs:	
Sonication Temperature (°C)	20-50
Ultrasound Intensity (w.cm^{-2})	12, 27, 48, 75, 108, 147, 192, 243, 300
Ultrasonic Irradiation time (min)	5-30
Outputs:	
Methanol Conversion (%)	70-100
Light Olefins Content (wt%)	36-84
Life Time (min)	50-540

Table 3

Learning rule	No. of neurons	R^2				MSE			
		Methanol conversion	Light Olefins content	Life time	Mean	Methanol conversion	Light Olefins content	Life time	Mean
LM	5	0.9808	0.9712	0.8308	0.9276	0.0045	0.0058	0.0204	0.0102
	10	0.9932	0.9759	0.9839	0.9843	0.0017	0.0049	0.0020	0.0029
	15	0.9957	0.9760	0.9929	0.9882	0.0010	0.0059	0.0009	0.0026
BR	5	0.9907	0.9756	0.9917	0.9860	0.0022	0.0049	0.0009	0.0027
	10	0.9957	0.9796	0.9922	0.9892	0.0010	0.0042	0.0009	0.0020
	15	0.9949	0.9538	0.9523	0.9670	0.0013	0.0094	0.0080	0.0062
SCG	5	0.9846	0.9673	0.9037	0.9519	0.0036	0.0065	0.0109	0.0070
	10	0.9904	0.9751	0.9397	0.9684	0.0022	0.0049	0.0069	0.0047
	15	0.9782	0.9606	0.8143	0.9177	0.0052	0.0080	0.0239	0.0123
RP	5	0.7583	0.8336	0.7886	0.7935	0.0580	0.0332	0.0260	0.0391
	10	0.8849	0.8121	0.7781	0.8250	0.0267	0.0377	0.0250	0.0298
	15	0.8146	0.8671	0.713	0.7982	0.0450	0.0274	0.0327	0.0350

Table 4

No. of Run	R^2				MSE			
	Methanol conversion	Light Olefins content	Life time	Mean	Methanol conversion	Light Olefins content	Life time	Mean
1	0.9999	1.0000	1.0000	1.0000	0.0002	0.0009	0.0008	0.0006
2	0.9998	0.9171	0.9564	0.9717	0.0001	0.0031	0.0010	0.0014
3	0.9994	0.9983	0.9998	0.9992	0.0001	0.0008	0.0007	0.0005
Mean	0.9997	0.9718	0.9854	**0.9856**	0.0001	0.0016	0.0008	**0.0008**

Table 5

Method	R^2				MSE			
	Methanol conversion	Light Olefins content	Life time	Mean	Methanol conversion	Light Olefins content	Life time	Mean
MLR	0.7005	0.7411	0.5121	0.6512	60.7065	68.1923	9207.9348	3112.2779
ANN	0.9957	0.9796	0.9922	0.9892	0.0010	0.0042	0.0009	0.0020

Table 6

No.	Ultrasonic Intensity (W/cm^2)	Ultrasonic Irradiation time (min)	Sonication Temperature (°C)	Methanol Conversion (%)	Light Olefins content (wt %)	Life time (min)
1	300	25	29	100	92	486
2	300	22	29	100	87	515
3	300	22	30	100	90	496
4	243	23	31	95	72	583
5	243	23	30	93	68	668
6	243	22	31	95	71	615
7	243	21	30	90	63	706
8	243	20	33	95	73	531
9	243	14	48	97	70	521
10	192	13	48	96	65	546

Table 7

Test No.	Ultrasonic Intensity (W/cm^2)	Ultrasonic Irradiation time (min)	Sonication Temperature (°C)	Methanol Conversion (%)		Light Olefins content (wt %)		Life time (min)	
				Experimental	Predicted	Experimental	Predicted	Experimental	Predicted
1	300	25	29	100	100	86	92	495	486
2	243	23	30	90	93	74	68	655	668
3	243	14	48	98	97	76	70	535	521